Astrochemistry: From Molecular Clouds to Planetary Systems
IAU Symposium, Vol. 197, 2000
Y. C. Minh and E. F. van Dishoeck, eds.

First Results from the Submillimeter Wave Astronomy Satellite – H_2O and O_2 Discoveries

Gary J. Melnick

Harvard-Smithsonian Center for Astrophysics, 60 Garden Street, Cambridge, MA 02138, USA

Abstract. The Submillimeter Wave Astronomy Satellite (*SWAS*) was successfully launched on 5 December 1998 with the goals of studying: (1) the distribution of oxygen in the interstellar medium; (2) the role of H_2O and O_2 as gas coolants; and (3) the UV-illuminated surfaces of molecular clouds. To achieve these goals, *SWAS* is conducting pointed observations of dense ($n(H_2) > 10^3$ cm^{-3}) molecular clouds throughout our Galaxy in either the ground-state or a low-lying transition of five astrophysically important species: H_2O, $H_2^{18}O$, O_2, CI, and ^{13}CO. *SWAS* has made great strides in each of these areas of investigation. This paper will summarize our H_2O and O_2 findings one year into the mission.

1. Introduction

A determination of the composition of the interstellar medium is of great interest for a variety of reasons, not least of which are the needs to fill significant gaps in our understanding of astrochemical processes and establish the influence different atoms and molecules may have on the early stages of star formation. The goal of the *SWAS* mission is to investigate these various aspects of star formation by focusing on a few key species. Table 1 lists the five species observed by *SWAS* in order of transition frequency. By observing O_2, H_2O, and $H_2^{18}O$, *SWAS* addresses two questions central to our understanding of molecular cloud chemistry and thermal balance: (1) "Where is all of the oxygen in the interstellar medium?" and (2) "Are water and, in some cases, O_2 dominant cloud coolants?" By observing CI and ^{13}CO, *SWAS* is able to study the UV-illuminated surfaces of molecular clouds. The relative strength and distribution of these two species offer important insights into the clumpiness of the gas, the stratification of atomic and molecular gas, and the gas temperatures.

Unfortunately, strong and pressure broadened terrestrial atmospheric features, even at mountain-top sites, effectively block almost all Galactic H_2O and O_2 emission. To overcome this obstacle, spectrometers onboard *ISO* have been used to study gas-phase H_2O. However, because *ISO* operated at wavelengths shortward of 200 microns and was only able to detect water vapor transitions that lie more than 80 K above the ground-state, it was primarily sensitive to gas warmer than that found throughout the bulk of dense molecular clouds. Thus, in most cases, it is hard to know whether the *ISO*-determined water abundances are representative of such clouds or if these results are affected by water liberated from grain mantles or chemical processing not favored at lower temperatures. Similarly, the *ISO* band (2.5–200μm) contained many O_2 transitions. However,

Table 1. Spectral lines observed by *SWAS*.

Species	Transition	Energy Above Ground State (E/k)	Frequency (GHz)	Critical Density (cm^{-3})
O_2	3,3–1,2	26 K	487.249	10^3
CI	$^3P_1$–$^3P_0$[a]	24 K	492.161	10^4
$H_2^{18}O$	1_{10}–1_{01}[a]	26 K	547.676	10^9[b]
^{13}CO	J=5–4	79 K	550.926	3×10^5
H_2O	1_{10}–1_{01}[a]	27 K	556.936	10^9[b]

[a] Ground-state transition.
[b] The critical density for H_2O will likely be less than this value by a factor of 10^2–10^4 due to significant radiation trapping in this line. The critical density for $H_2^{18}O$ could be reduced by a factor of 1.5–50 due to the same effect.

these transitions all lie more than 180 K above the ground-state and within molecular clouds the column density in any one of these lines would be expected to be quite small and undetectable by *ISO*.

For the first time, *SWAS* permits the opportunity to observe transitions of gaseous H_2O and O_2 whose energy above the ground-state (see Table 1) is well-matched to the temperatures typical of molecular clouds. Moreover, *SWAS* allows examination of a large number of lines-of-sight throughout the Galaxy. In addition, the $\lesssim 1$ km s^{-1} spectral resolution of *SWAS* (versus $\gtrsim 10$ km s^{-1} for *ISO*) allows *SWAS* to measure line profiles sufficiently well to distinguish between emission from outflows and shocked gas and more quiescent regions.

The observing strategy for *SWAS* is twofold: (1) to establish the presence of, or set a scientifically interesting abundance upper limit on H_2O and O_2, and (2) to map the large-scale distributions of CI and ^{13}CO. Since little is known about the H_2O distribution and even less is known about the O_2 abundance and distribution, more than half of the mission will be devoted to searching for and mapping the distributions of these species. The remainder of the three-year baseline mission will be dedicated to conducting large-scale ($\sim 1^\circ \times 1^\circ$) CI and ^{13}CO mapping toward approximately 20 specifically interesting clouds.

Section 2 of this paper will provide an overview of the mission. Section 3 will review some of early results of the mission as they apply to the H_2O and O_2 questions raised above. Reference will be made to a number of *SWAS* first light papers that will soon appear in the *Astrophysical Journal Letters*; the interested reader is encouraged to review these papers for more background and detail than is possible to present here.

2. Mission Overview

SWAS is a complete radio observatory in space, including a 54×68-cm off-axis Cassegrain telescope along with two independent Schottky barrier diode mixers, passively cooled to ~ 175 K. Receiver 1 is used to observe O_2 at 487 GHz and

Table 2. *SWAS* instrument summary.

Telescope:	54×68 cm Diameter Off-Axis Cassegrain
Aperture Efficiency	66%
Main Beam Efficiency	90%
Beamsize:	3.5×5.0 arcminutes @ 490 GHz
	3.3×4.5 arcminutes @ 553 GHz
Absolute Pointing Accuracy:	≤ 5 arcseconds (1σ)
Jitter:	≤ 5 arcseconds (1σ)
Receiver Type:	Schottky Barrier Diode Harmonic Mixers
Receiver Noise Temperature:	2500 K (DSB) Receiver 1 (O_2, CI)
	2200 K (DSB) Receiver 2 (^{13}CO, H_2O)
	4000 K (DSB) Receiver 2 ($H_2{}^{18}O$)
Backend Spectrometer:	1.4 GHz Bandwidth ($\Leftrightarrow 840$ km s^{-1}) AOS
Velocity Resolution:	0.6 km s^{-1}
Orbit:	650 km; 70° Inclination
Mission Lifetime:	≥ 3 years

CI at 492 GHz in the lower and upper sidebands, respectively. Receiver 2 is used to observe ^{13}CO at 551 GHz and H_2O at 557 GHz in the lower and upper sidebands, respectively. The ground-state transition of ortho-$H_2{}^{18}O$ at 548 GHz is observed by tuning Receiver 2 slightly beyond its nominal operating range which results in about two times higher system noise temperature. With the use of a 1.4 GHz bandwidth acousto-optical spectrometer (AOS), *SWAS* has the ability to simultaneously observe either the H_2O, O_2, CI, and ^{13}CO lines *or* the $H_2{}^{18}O$, O_2, and CI lines. To ensure that the *SWAS* spectral lines are centered in the AOS, regardless of their $v_{\rm LSR}$ within the Galaxy, Receivers 1 and 2 are tunable over ± 182 and ± 164 km s^{-1}, respectively. Table 2 presents a summary of key instrument parameters.

SWAS was launched into a 650 km, 70° inclination circular orbit from which it conducts observations in a "point and integrate" mode. As *SWAS* orbits the Earth, sources become visible outside of the 75° Sun and 45° Earth limb avoidance angles. *SWAS* initially acquires and then inertially points toward a source until either a higher priority source becomes available or an avoidance angle is approached. *SWAS* typically observes two to four sources per 97-minute orbit. For purposes of mapping or long integrations, *SWAS* can return to a given source on successive orbits, accumulating as much as ~ 10 hours of observing time on a single position per day.

With the exception of a few sources – notably stars and Jupiter – all observations have been conducted by nodding the entire observatory (vs. use of the chopping secondary mirror). This approach ensures that good reference positions are always used and, because there is no change in the optical path between ON-source and OFF-source reference observations, the spectral baselines are generally very flat. Reference positions can be up to 3° from the ON-source position in any direction and are selected for each source to coincide with the closest position exhibiting no detectable ^{12}CO J=1–0 emission. A complete description of the instrument, data taking procedures, and data products can be found in Melnick et al. (2000).

3. Early Science Results

3.1. Distribution and abundance of H_2O

In the subsections below, the inferred water abundances toward quiescent clouds, outflow regions, and Sgr B2 are presented. As a guide to the discussion to follow, the Figure 1 *left* panel shows the predicted time-dependent abundances of H_2O and O_2, along with C and CO, in regions shielded from dissociating UV radiation. A modification to this model, depicted in the Figure 1 *right* panel, will be discussed in Section 4.

H_2O in Quiescent Clouds – Orion Ridge, M17 SW, S140, ρ Oph, B335: The $1_{10}-1_{01}$ transition of H_2O has a high critical density ($\Leftrightarrow 3 \times 10^8$ cm^{-3} at 20 K and 8×10^7 cm^{-3} at 40 K) and is expected to have a high optical depth even for relatively small water abundances. Thus, trapping plays an important role in the excitation of this transition. For large optical depths, the "effective critical density" is approximately $A_{u\ell}/\tau_o C_{u\ell}$, where $A_{u\ell}$ is the spontaneous emission rate, τ_o is the line-center optical depth, and $C_{u\ell}$ is the collisional de-excitation rate. In the regime where $n(H_2) \ll n_{crit.(eff)}$ or, equivalently, $T_B \ll (h\nu/4k)\, e^{-h\nu/kT}$ (see Linke et al. 1977):

$$\int T_B\, dv \;=\; C_{u\ell} \left(\frac{h\nu}{4\pi}\right) \left(\frac{c^3}{2k\nu^3}\right) e^{-h\nu/kT}\, N(\mathrm{o-H_2O})\, n(\mathrm{H_2}) \qquad (1)$$

or

$$x(\mathrm{o-H_2O}) \;=\; f(T)\, \frac{\int T_B\, dv}{N(\mathrm{H_2})\, n(\mathrm{H_2})}\;, \qquad (2)$$

where $x(\text{o-H}_2\text{O}) \equiv n(\text{o-H}_2\text{O})/n(\text{H}_2)$ and $f(T) = e^{h\nu/kT}/C_{u\ell}$. Collision rate coefficients are obtained from Phillips et al. (1996). The antenna temperature, T_A, which is directly measured by *SWAS*, is related to the brightness temperature, T_B, via the expression $T_A = T_B$ (cloud size/beam size)^2. At a temperature of 40 K, the 557 GHz water line is effectively thin if the antenna temperature is less than ~ 3.5 K. In M17 SW, S140, ρ Oph, and most positions in Orion, the maximum observed intensity for the H_2O emission is less than 0.5 K (after correction for the *SWAS* main beam efficiency). Therefore, unless the beam filling factor is quite small, the emission in the regions discussed here is effectively thin and Eqn. (2) applies.

The temperature, T, H_2 column density, $N(H_2)$, the H_2 volume density, $n(H_2)$, and the cloud size are determined from ground-based measurements (see Snell et al. 2000*a*, *b*; Ashby et al. 2000). In all cases, these ground-based measurements have been obtained with both beamsizes and spatial sampling small compared to the *SWAS* beamsize. By varying the assumed o-H_2O abundance, computing the resultant o-H_2O line intensity at each grid point, spatially convolving the results to match the *SWAS* beamsize, and comparing the integrated

https://doi.org/10.1017/S0074180900164769 Published online by Cambridge University Press

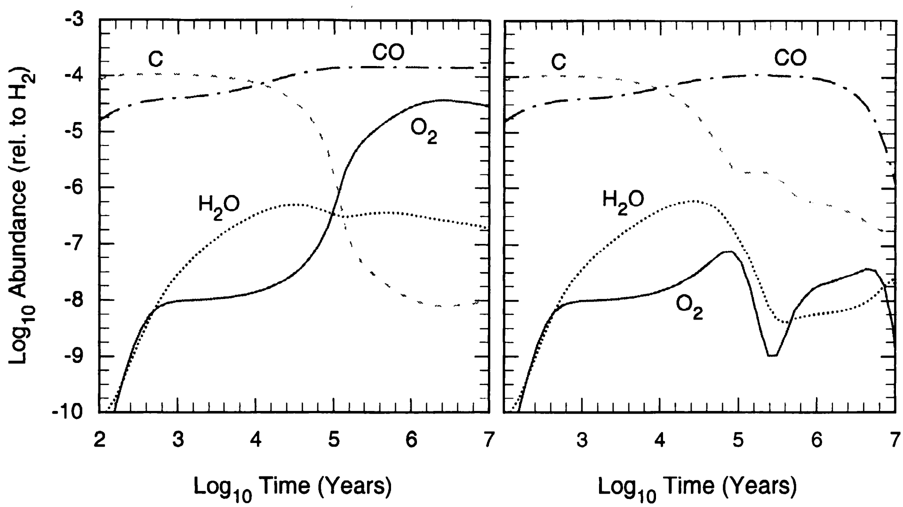

Figure 1. Results of time-dependent chemical models for $n(\mathrm{H}_2) = 10^5$ cm^{-3}, $T_{\mathrm{gas}} = T_{\mathrm{dust}} = 30$ K and $A_{\mathrm{V}} = 20^{\mathrm{m}}$. The model shown in the *left* panel includes depletion and desorption onto grain surfaces, but no surface chemistry. The model shown in the *right* panel includes depletion and desorption onto grain surfaces, but with simple surface chemistry (after Bergin et al. 2000).

intensity to the measured $\int T_A\,dv$ it is possible to iteratively converge on the values of $x(\text{o-H}_2\text{O})$ that reproduce the *SWAS* observations. This method of modeling naturally accounts for variations in physical parameters across the *SWAS* beam and also correctly accounts for the coupling of the *SWAS* beam to the source. The results are presented in Table 3.

In addition to the $1_{10}-1_{01}$ H_2O transition, *SWAS* has also obtained useful upper limits on the strength of the $1_{10}-1_{01}$ $H_2^{18}O$ transition toward many of the same lines-of-sight. Figure 2 shows one such example toward M17 SW. The upper limits to the ortho-water abundances thus inferred are in generally good agreement with the values given in Table 3 for quiescent clouds and suggest that resonant line scattering is not a strong effect. Similarly, Monte Carlo calculations that include the effects of a dust continuum (Ashby et al. 2000) indicate that ignoring the far-infrared radiation field has a small impact on the derived water abundance.

H_2O in Outflow Regions – NGC 2071, L1157, NGC 1333 (IRAS 4): In contrast to the narrow, often single-peaked, water lines observed from quiescent gas, *SWAS* observations of the above objects reveal broad ($\gtrsim 30$ km s^{-1} FWZP) emission (accompanied by a narrow absorption feature at the velocity of the quiescent gas) suggesting that the water emission in all three sources is associated with gas in the outflow. In order to obtain a rough estimate of the water abundance, the mass of the outflow gas and its typical density and temperature need to be known.

https://doi.org/10.1017/S0074180900164769 Published online by Cambridge University Press

Table 3. Inferred ortho-H_2O abundances.

Source	$[o-H_2O] / [H_2]$		Ref.
Quiescent Regions:			
M17 SW	$2\text{–}4 \times 10^{-9}$	(6 positions)	a
Orion (3.2′ S of BN/KL)	4×10^{-8}		b
S140	1.6×10^{-8}		c
ρ Oph A	6×10^{-8}		c
B335	$< 3.5 \times 10^{-6}$ (3σ)		c
Outflow Regions:			
NGC 2071	5×10^{-7}		d
L1157	1.5×10^{-6}		d
NGC 1333 (IRAS 4)	1.6×10^{-6}		d
Sgr B2:			
$-108 \leq v_{LSR} \leq -74$ km s^{-1}	0.8×10^{-6}		e
$-74 \leq v_{LSR} \leq -50$ km s^{-1}	$> 0.2 \times 10^{-6}$		e
$-50 \leq v_{LSR} \leq -10$ km s^{-1}	1.1×10^{-6}		e
$-10 \leq v_{LSR} \leq +20$ km s^{-1}	1.0×10^{-6}		e

Ref. - [a]Snell et al. 2000*a*. [b]Snell et al. 2000*b*. [c]Ashby et al. 2000. [d]Neufeld et al. 2000*a*. [e]Neufeld et al. 2000*b*.

Mass estimates have been derived from observations of CO emission from the outflows, together with assumptions about the CO rotational temperature and the CO/H_2 ratio (the latter usually taken to be 10^{-4}). Temperature and density estimates have been obtained from multitransition studies of $H^{13}CO^+$ (Wootten et al. 1984) and NH_3 (Takano et al. 1986) in the case of NGC 2071, CS (Mikami et al. 1992) and NH_3 (Tafalla & Bachiller 1995) for L1157, and H_2CO (Blake et al. 1995) for NGC 1333 IRAS 4. Table 4 summarizes these results.

Using these estimates of the mass, mean density, and mean temperature for each outflow, a simple single-component model can be used to obtain a very rough estimate of the water abundance from the *SWAS* observations of the H_2O $1_{10}-1_{01}$ line strengths. It is expected that this transition is *effectively thin*, although optically thick, such that each collisional excitation from 1_{01} to 1_{10} is followed by a radiative decay. With this assumption, Eqn. (2) can be rewritten:

$$x(o-H_2O) \;=\; 2 \times 10^{-5}\, \frac{d_{\rm kpc}^2}{n_5\, M\, q_{-11}} \int T_A\, dv/{\rm K\ km\ s^{-1}} \qquad (3)$$

where $d_{\rm kpc}$ is the source distance in kpc, $10^5\, n_5$ cm^{-3} is the H_2 density, M is the outflow mass in solar units, and $10^{-11}\, q_{-11}$ cm^3 s^{-1} is the rate coefficient for excitation from the 1_{01} to the 1_{10} level (Phillips et al. 1996).

Clearly, this approach has its drawbacks as it assumes global values for the density and temperature. In reality, each outflow is undoubtedly marked by a range of temperatures and densities. Unfortunately, the ancillary data needed

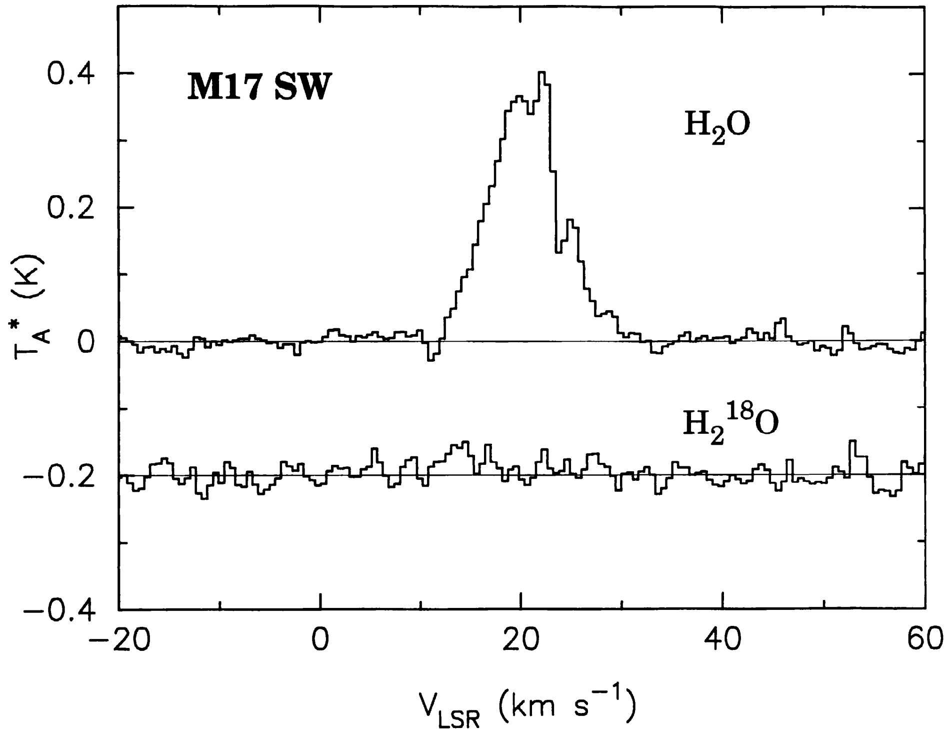

Figure 2. *SWAS*-obtained spectra of the 1_{10}–1_{01} H_2O and $H_2^{18}O$ lines toward the center of the M17 cloud core (from Snell et al. 2000*a*).

to construct a more realistic model do not exist. Table 3 lists the derived ortho-water abundance for each source.

H_2O Toward Sgr B2: *SWAS* was used to observe the $1_{10}-1_{01}$ transition of both $H_2^{16}O$ and $H_2^{18}O$ toward Sgr B2. As is shown in Figure 3, the spectra show a complex pattern of absorption and – in the case of $H_2^{16}O$ – emission, with numerous features covering a wide range of LSR velocities (−130 to +130 km s^{-1}) and representing absorption both in gas associated with Sgr B2 as well as by several components along the line-of-sight. The range of velocities for which absorption is observed in the $H_2^{16}O$ line agrees qualitatively with the *ISO* spectrum of the $H_2^{16}O$ $2_{12}-1_{01}$ line obtained previously at much lower spectral resolution by Cernicharo et al. (1997).

A quick inspection of the spectrum in Figure 3 shows immediately that for LSR velocities ≤ 20 km s^{-1}, the $H_2^{16}O$ flux falls close to zero whenever there is detectable absorption in the $H_2^{18}O$ line. For an assumed $H_2^{16}O : H_2^{18}O$ abundance ratio > 200, this behavior is expected provided: (1) that the absorbing gas completely covers the submillimeter continuum source; and (2) that the $H_2^{16}O$ $1_{10}-1_{01}$ transition has a negligible excitation temperature. Since the critical density for this transition is $\sim 10^8$ cm^{-3} for $T \sim 20$–40 K, a low excitation temperature is expected except in dense cores or radiatively-pumped regions. For

https://doi.org/10.1017/S0074180900164769 Published online by Cambridge University Press

Table 4. Properties and observational results for outflow sources[a]

Source	Distance (pc)	$\int T_A(1_{10}–1_{01})dv$ (K km s^{-1})	$n(H_2)$ (cm^{-3})	Mass ($M_\odot$)	Temp. (K)
NGC 2071	390	3.11	4×10^5	7.1	33
L1157	440	1.34	3×10^5	0.72^b	80
NGC1333 IRAS4	350	1.27	5×10^{6b}	$0.025^{b,c}$	80

[a] After Neufeld et al. (2000*a*).
[b] Inner outflow region only.
[c] CO emission assumed optically thin.

LSR velocities between +20 and +90 km s^{-1} the $H_2{}^{16}O$ flux is greater than zero even in the presence of strong $H_2{}^{18}O$ absorption implying that the $H_2{}^{16}O$ is significantly excited in either very dense gas or by radiative pumping or that the absorbing gas does not fully cover the submillimeter continuum source.

The $H_2{}^{18}O$ absorption shows a structure broadly similar to that observed in many molecular species, the interpretation of which has been summarized by Greaves (1995). Based on that interpretation, the LSR velocity range between −130 and +20 km s^{-1} is divided into 4 separate intervals shown in Figure 3. The first two intervals, (−108, −74) and (−74, −50) km s^{-1}, show absorption that is believed to arise in gas lying within 1 kpc of the Galactic Center. The third interval, (−50, −10) km s^{-1}, shows absorption that originates in foreground gas at Galactocentric radii $\sim$3–5 kpc, while the fourth interval, (−10, +20) km s^{-1}, shows absorption due to gas within a few hundred pc of the Sun as well as gas within spiral arms at Galactocentric radii $\sim$5–8 kpc.

The column density of $H_2{}^{16}O$ or, when the $H_2{}^{16}O$ flux is zero, the $H_2{}^{18}O$ column density can be determined directly from the absorption spectra. To derive estimates of the water abundances, the column density of H_2 present in the various v_{LSR} intervals must be determined. To do this, use was made of the ^{13}CO spectrum of Sgr B2 obtained by Bally et al. (1988) along with the assumption that the $^{12}CO/^{13}CO$ and $H_2{}^{16}O/H_2{}^{18}O$ abundance ratios are 30 and 250, respectively, for gas at v_{LSR}'s between −108 and −10 km s^{-1}, and 60 and 500, respectively, for gas at v_{LSR}'s between −10 and +20 km s^{-1} (e.g. Langer & Penzias 1990). It is also assumed that the $^{12}CO/H_2$ abundance ratio is 10^{-4} in all v_{LSR} intervals. The ortho-H_2O abundances thus inferred are listed in Table 3.

The spectra for $v_{LSR} \geq +20$ km s^{-1} – interval 5 in Figure 3 – show absorption (and emission) believed to arise within gas associated with Sgr B2. The $H_2{}^{18}O$ spectrum is consistent with that obtained by Zmuidzinas et al. (1995), which can be accounted for by assuming gas temperatures less than 90 K and an $H_2{}^{16}O$ abundance of 2×10^{-7} (Zmuidzinas et al. 1995). However, this abundance results in much stronger $H_2{}^{16}O$ emission in the v_{LSR} interval (+90, +120) km s^{-1} than observed. This discrepancy can be reconciled if a diffuse envelope of gas, larger than the *SWAS* beam, scatters much of the $H_2{}^{16}O$ emission out of the line-of-sight.

https://doi.org/10.1017/S0074180900164769 Published online by Cambridge University Press

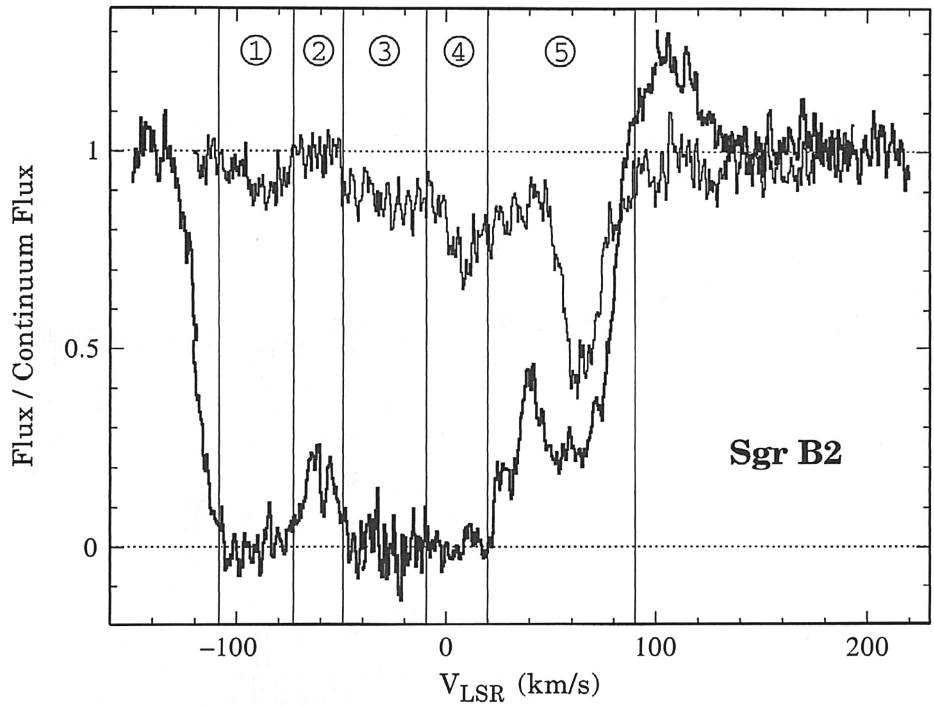

Figure 3. Water vapor spectra obtained toward Sagittarius B2 by *SWAS*. The figure shows the $1_{10}-1_{01}$ pure rotational transition of $H_2{}^{16}O$ near 557 GHz (heavy line) and the analogous line of $H_2{}^{18}O$ near 548 GHz (lighter line) (adapted from Neufeld et al. 2000*b*). The different velocity components discussed in the text are appropriately shaded.

3.2. O_2 in molecular clouds

As shown in Figure 1 (*left* panel), time-dependent chemical models (e.g. Graedel et al. 1982; Bergin et al. 1995) predict that in the absence of a photodissociating UV field, the abundance of O_2 will begin to exceed 10^{-5} approximately 3×10^5 years after the initiation of molecular chemistry. Abundances this high would make O_2 an important gas coolant (Goldsmith & Langer 1978; Neufeld et al. 1995).

Because the magnetic dipole transition that gives rise to $N_J=3_3-1_2$ line is inherently weak, it is highly likely that this line is optically thin. Moreover, the effects of far-infrared and submillimeter continuum emission can be ignored. The integrated intensity observed (corrected for the main beam efficiency) is then proportional to the column density in the upper level of the transition:

$$\int T_A\, dv \;=\; \frac{A_{u\ell} h c^3}{8\pi k \nu^2}\, \mathrm{N}(O_2)\, f_u \tag{4}$$

where $A_{u\ell}$ is the spontaneous decay rate, $\mathrm{N}(O_2)$ is the total O_2 column density, and f_u is the fractional population of the upper 3_3 level. To obtain the O_2

https://doi.org/10.1017/S0074180900164769 Published online by Cambridge University Press

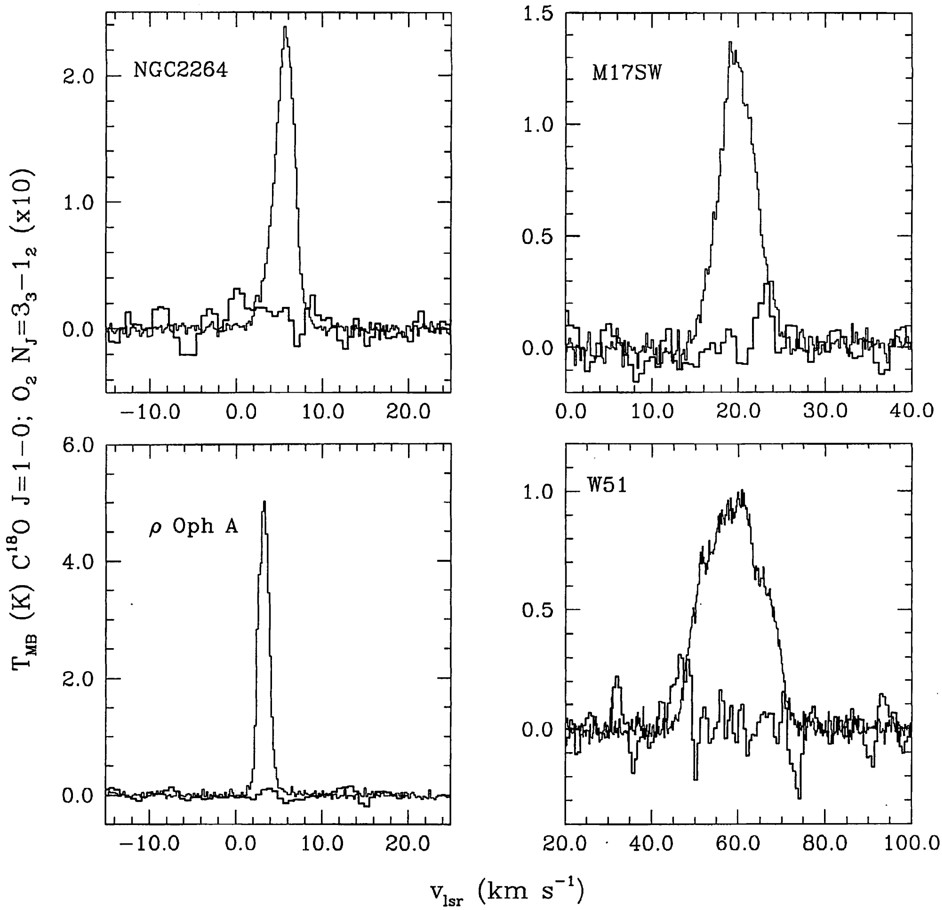

Figure 4. Spectra of the N_J=3_3−1_2 transition of O_2 (heavy lines) and the J=1→0 transition of $C^{18}O$ (light lines) toward four regions (after Goldsmith et al. 2000).

abundance relative to H_2, it is useful to first establish the abundance of O_2 relative to a molecule with similar properties – optically thin, similar A coefficients, close to LTE, and insensitive to background continuum – and whose abundance relative to H_2 is believed to be understood. These criteria are met by J=1→0 transition of $C^{18}O$ transition (see Goldsmith et al. 2000). The ratio of column densities is then:

$$\frac{\mathrm{N(O_2)}}{\mathrm{N(C^{18}O)}} = \left[\frac{\nu^2_{\mathrm{O_2}}\, A_{\mathrm{C^{18}O}}}{\nu^2_{\mathrm{C^{18}O}}\, A_{\mathrm{O_2}}}\right] \times \left[\frac{f_u\,(\mathrm{C^{18}O})}{f_u\,(\mathrm{O_2})}\right] \times \left[\frac{\int T_A\,(\mathrm{O_2})\, dv}{\int T_A\,(\mathrm{C^{18}O})\, dv}\right]$$

$$= 155.5 \times \mathrm{R_{CF}} \times \mathrm{R_T} \qquad (5)$$

https://doi.org/10.1017/S0074180900164769 Published online by Cambridge University Press

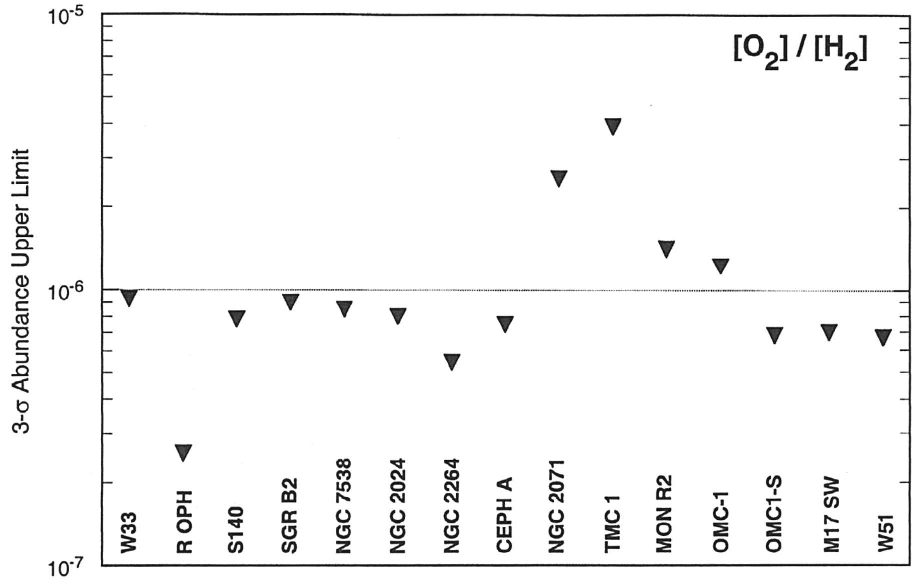

Figure 5. Current *SWAS*-established $3\,\sigma$ upper limits to the gas-phase O_2 abundance toward a sample of Galactic molecular clouds (adapted from Goldsmith et al. 2000).

where the ratio of correction factors, R_{CF}, is the ratio of fractional populations in the $C^{18}O$ J=1 and the O_2 N_J=3_3 levels and R_T is the ratio of integrated main beam temperatures. As shown in Goldsmith et al. (2000), for conditions expected to apply in GMC cores, $n(H_2) \geq 10^{4.5}$ cm^{-3} and $25 \leq T \leq 40$ K, R_{CF} ranges between values of 1.3 and 2.2. In cooler ($10 \leq T \leq 25$ K) dark cloud cores, R_{CF} has a larger range – between about 2.2 and 8.0.

Deep integrations in the O_2 $N_J = 3_3$–1_2 line have been carried out by *SWAS* toward a variety of Galactic molecular clouds with no convincing detections to report (see Figure 4). Figure 5 shows the 3σ upper limits to the O_2 abundance as of Fall 1999.

4. Constraints Upon and Paths to a Comprehensive Model

Two things are clear from the results presented in Table 3 and Figure 5. First, gaseous H_2O and O_2 are not primary carriers of elemental oxygen in molecular clouds. Second, as a result, H_2O and O_2 are not significant coolants of quiescent molecular gas. More specifically, the *SWAS* results require that any successful model not only accounts for values of $[O_2]/[H_2] \lesssim 7 \times 10^{-7}$, but also for low ortho-water abundances toward dense star-forming regions while simultaneously allowing for higher ortho-water abundances found in outflow sources and the low density gas along the line-of-sight to Sgr B2. In addition, a successful model must: (1) account for the co-existence in the gas-phase of complex carbon-bearing species, such as HC_3N, HCN, and CH_3C_2H, with simple and complex oxygen-bearing species, such as SO and CH_3OH; (2) have water-ice abundances as high as 10^{-4}; and, (3) do all of the above without asserting enhanced penetration of UV radiation as this would conflict with the existence of many other molecules (e.g. NH_3) with photo-destruction rates similar to H_2O and O_2.

Among the solutions considered, two show some promise in meeting these constraints. First, an enhanced gas-phase C/O ratio would suppress the gas-phase production of H_2O and O_2 while leaving the carbon chemistry largely unaffected. Such an enhancement could occur as a result of grain surface chemistry (e.g. Blake et al. 1987). Specifically, if instead of oxygen atoms depleting onto grains, remaining inert, and eventually evaporating – the case depicted in the *left* panel of Figure 1 – two surface reactions are included ($O + gr \rightarrow H_2O(gr)$ and $C + gr \rightarrow CH_4(gr)$) then the results depicted in the *right* panel of Figure 1 are predicted (Bergin et al. 2000). The water produced on the grains will not evaporate so long as $T_{dust} < 90$ K, whereas CH_4 is quite volatile and is released into the gas-phase thus enhancing the carbon chemistry. Further, because the depletion timescales are longer at lower densities, the inclusion of grains naturally allows for a difference between the higher water abundances found toward Sgr B2 and the lower water abundances observed in star-forming regions. The higher water abundances also observed toward outflow sources are likely the result of the vaporization of water-ice on grain mantles and the increased water production via neutral-neutral reactions, both due to shock heating.

Figure 1 also shows that low H_2O and O_2 abundances prevail at times early in the chemical evolution of a cloud. A second class of solutions would maintain the chemical youth of chronologically old clouds through the dynamical cycling of atomic and ionized species at the surface into molecular gas deeper within a cloud. It has been shown that the H_2O and O_2 abundances can be lowered by several orders of magnitude below steady state values by the inclusion of enhanced amounts of H^+, He^+, C^+, and C in the dense well-shielded interiors (e.g. Chièze & Pineau des Forêts 1989; Xie et al. 1995). The challenge now ahead of both possible solutions is to include gas-grain interactions and investigate the abundances of a large number of observed species.

References

Ashby, M.L.N., et al. 2000, in preparation
Bally, J., Stark, A.A., Wilson, R.W., & Henkel, C. 1988, ApJ, 324, 223
Bergin, E.A., Langer, W.D., & Goldsmith, P.F. 1995, ApJ, 441, 222
Bergin, E.A., et al. 2000, submitted to ApJ Letters
Blake, G.A., Sandell, G., van Dishoeck, E.F., Groesbeck, T.D., Mundy, L.G., & Aspin, C. 1995, ApJ, 441, 689
Blake, G.A., Sutton, E.C., Masson, C.R., & Phillips, T.G. 1987, ApJ, 482, 285
Cernicharo, J., et al. 1997, A&A, 323, L25
Chièze, J.P. & Pineau des Forêts, G. 1989, A&A, 221, 89
Goldsmith, P.F. & Langer, W.D. 1978, ApJ, 221, 881
Goldsmith, P.F. et al. 2000, to appear in ApJ Letters
Graedel, T.E., Langer, W.D., & Frerking, M.A. 1982, ApJS, 48, 321
Greaves, J.S. 1995, MNRAS, 273, 918
Langer, W.D. & Penzias, A.A. 1990, ApJ, 357, 477

Linke, R.A., Goldsmith, P.F., Wannier, P.G., Wilson, R.W., & Penzias, A.A. 1977, ApJ, 214, 50
Melnick, G.J., et al. 2000, to appear in ApJ Letters
Mikami, H., Umemoto, T., Yamamoto, S., & Saito, S. 1992, ApJ, 392, L87
Neufeld, D.A., et al. 2000*a*, to appear in ApJ Letters
Neufeld, D.A., et al. 2000*b*, to appear in ApJ Letters
Neufeld, D.A., Lepp, S., & Melnick, G.J. 1995, ApJS, 100, 132
Phillips, T.R., Maluendes, S., & Green, S. 1996, ApJS, 107, 467
Snell, R.L., et al. 2000*a*, in preparation
Snell, R.L., et al. 2000*b*, submitted to ApJ Letters
Tafalla, M. & Bachiller, R. 1995, ApJ, 443, L37
Takano, T., Stutzki, J., Winnewisser, G., & Fukui, Y. 1986, A&A, 167, 333
Wootten, A., Loren, R.B., Sandqvist, Å., Friberg, P., & Hjalmarson, Å. 1984, ApJ, 279, 633
Xie, T., Allen, M., & Langer, W.D. 1995, ApJ, 440, 674
Zmuidzinas, J., Blake, G.A., Carlstrom, J., Keene, J., Miller, D., Schilke, P., & Ugras, N.G. 1995, in Galactic Ecosystem: From Gas to Stars to Dust, eds. M.R. Haas, J.A. Davidson, & E.E. Erickson, ASP, 33

https://doi.org/10.1017/S0074180900164769 Published online by Cambridge University Press

Discussion

W. A. Schutte: How do the high abundances of atomic O as observed e.g. by Caux et al. (this conference) modify your interpretation of the low gaseous abundances of O_2 and H_2O ?

G. J. Melnick: The SWAS and the O I absorption results are not in apparent disagreement. It may be that along many lines-of-sight most of the elemental oxygen is in the form of gaseous atomic oxygen and in water-ice on grain mantles (and not in the form of gaseous O_2 or H_2O).

D. A. Williams: Thank you for these beautiful results. The interpretation you give of freeze-out of species onto dust seems very plausible, but is it consistent with the assumption of uniform $C^{18}O/H_2$ which I understand you assumed in estimating abundances ?

G. J. Melnick: If you assume that some fraction of $C^{18}O$ is frozen onto grains, then the $[O_2]$/[total gas + ice $C^{18}O$] ratio decreases further. We measure the gas-phase $C^{18}O$ column density; if there is 'more' $C^{18}O$ in the form of ice, then the total $C^{18}O$ column density is underestimated in our analysis and ultimately the $[O_2]/[H_2]$ will be lower than the values I present here.

M. Guélin: Can you compare the limits you derive with SWAS on the molecular oxygen abundance with those which can be derived from the ground by observing the 1.3 mm $O^{18}O$ line (e.g. the recent observations of Combes et al. and Fuente et al.) ?

G. J. Melnick: The lowest limit SWAS has set to date is $N(O_2)/N(CO) \leq 0.0042$ ($3\,\sigma$) toward M17. The Combes, Wiklind, & Nakai (1997, A&A, 327, 453) result for absorption against the z=0.685 source was $N(O_2)/N(CO) \leq 0.006$ (3σ). If I recall correctly Fuente et al. (1993, A&A, 275, 558) find $N(O_2)/N(CO) \leq 0.1$. Hopefully, we will continue to improve - i.e. drive lower - the $N(O_2)/N(CO)$ limit as the SWAS mission progresses.

J. Crovisier: SWAS has also observed the water line in one comet (C/1999 H1 Lee). Could you give some details on this observation ? What are future projects to observe comets with SWAS ?

G. J. Melnick: SWAS observed Comet C/1999 H1 Lee over the period 1999 May 19.0 – 23.7 UT. The average integrated antenna temperature was 1.79 ± 0.03 $\mathrm{K\,km\,s^{-1}}$ within $3.3'\times4.5'$ (FWHM) beam. For an ortho : para water ratio of 3, our best estimate of the total water evaporation rate is 1.0×10^{29} $\mathrm{s^{-1}}$. Lastly, there is no evidence for any periodicity during the 4.7 days we monitored the comet. We plan to re-observe Comet Lee post-perihelion and we will certainly observe any other comets that should appear during the SWAS mission.

https://doi.org/10.1017/S0074180900164769 Published online by Cambridge University Press